

Perception Characteristics Distance: Measuring Stability and Robustness of Perception System in Dynamic Conditions under a Certain Decision Rule

Boyu Jiang^{1*} Liang Shi^{2*} Zhengzhi Lin¹ Loren Stowe² Feng Guo^{1,2†}

¹Department of Statistics, Virginia Tech, Blacksburg, VA 24061

²Virginia Tech Transportation Institute, Virginia Tech, Blacksburg, VA 24061

feng.guo@vt.edu

Abstract

The performance of perception systems in autonomous driving systems (ADS) is strongly influenced by object distance, scene dynamics, and environmental conditions such as weather. AI-based perception outputs are inherently stochastic, with variability driven by these external factors, while traditional evaluation metrics remain static and event-independent, failing to capture fluctuations in confidence over time. In this work, we introduce the Perception Characteristics Distance (PCD) — a novel evaluation metric that quantifies the farthest distance at which an object can be reliably detected, incorporating uncertainty in model outputs. To support this, we present the SensorRainFall dataset, collected on the Virginia Smart Road using a sensor-equipped vehicle (cameras, radar, LiDAR) under controlled daylight-clear and daylight-rain scenarios, with precise ground-truth distances to the target objects. Statistical analysis reveals the presence of change points in the variance of detection confidence score with distance. By averaging the PCD values across a range of detection quality thresholds and probabilistic thresholds, we compute the mean PCD (mPCD), which captures the overall perception characteristics of a system with respect to detection distance. Applying state-of-the-art perception models shows that mPCD captures meaningful reliability differences under varying weather conditions — differences that static metrics overlook. PCD provides a principled, distribution-aware measure of perception performance, supporting safer and more robust ADS operation, while the SensorRainFall dataset offers a valuable benchmark for evaluation. The **SensorRainFall dataset** is publicly available at <https://www.kaggle.com/datasets/datadrivenwheels/sensorrainfall>, and the evaluation **code is open-sourced at** https://github.com/datadrivenwheels/PCD_Python

1 Introduction

Perception systems—particularly object detection—are central to intelligent decision-making in AI-powered vision applications. In autonomous driving systems (ADS) and advanced driver-assistance systems (ADAS), they facilitate real-time comprehension and interaction with complex, dynamic environments. However, standard evaluation metrics such as mean average precision (mAP), Intersection-over-Union (IoU), and the F1 score are based on static, frame-level assessments. These metrics overlook the temporal and spatial continuity intrinsic to real-world scenarios, making them inadequate for evaluating the robustness of perception systems under dynamic operating conditions.

*These authors contributed equally to this work.

†Corresponding author

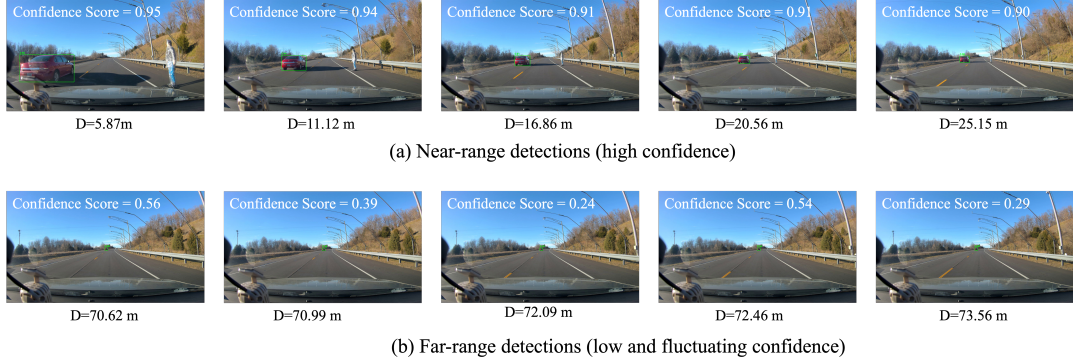


Figure 1: Comparison of detection confidence at near vs. far ranges. Near-range object detections with consistently high confidence scores (≥ 0.90). Far-range detections exhibit unstable and fluctuating confidence, including brief drops as low as 0.24. Despite visual continuity of the object, detection reliability degrades with increasing distance.

In practical ADS and ADAS deployments, control decisions often rely on threshold-based detection logic—i.e., if the model’s confidence score exceeds a fixed threshold, an object is considered detected; otherwise, it is not. However, such binary logic overlooks the stochastic and dynamic nature of perception outputs. Figure 1 illustrates this limitation using the performance of a YOLOX-based object detector at near-range (a) and far-range (b). As the ego vehicle follows a leading car on a highway, detection confidence fluctuates significantly at farther distances (≥ 70 m, Figure 1 (b)). These fluctuations challenge downstream control modules that depend on stable, high-confidence detections for safe acceleration or braking. Applying a fixed threshold (e.g., confidence score ≥ 0.4) results in inconsistent detection decisions, making the maximum reliable detection range ambiguous. This motivates the development of a dynamic evaluation framework that captures the spatial variability and distance-dependent reliability of perception systems under realistic conditions.

To address these challenges, we propose a novel evaluation metric—Perception Characteristics Distance (PCD)—which quantifies the maximum distance within which a perception system can consistently produce reliable detections at a given detection threshold. Unlike traditional static metrics, PCD accounts for the spatial dynamics of perception by statistically estimating the mean and variance of detection confidence as a function of distance. This probabilistic formulation enables PCD to robustly capture performance variability over time and space, offering a more accurate and context-aware assessment of system reliability under real-world conditions. To enable a comprehensive comparison, we define the mean PCD (mPCD) as the average of PCD values computed over a range of detection thresholds.

For benchmarking, we present the SensorRainFall dataset, which—to the best of the authors’ knowledge—is the only publicly available dataset collected in a highly controlled environment designed for perception evaluation in ADS and ADAS. Data was collected on the Virginia Smart Roads, a facility capable of simulating diverse weather conditions. All other environmental factors were held constant, with only the weather (clear vs. rainy) varying between scenarios. The dataset includes object-level annotations across multiple sensor modalities (camera, radar, LiDAR), with ground-truth bounding boxes manually reviewed and annotated for a red sedan in each frame.

2 Related works

Video datasets are vital for advancing autonomous driving perception by capturing real-world variability. nuScenes offers rich multimodal data for complex urban environments [1], while KITTI remains a foundational benchmark for object detection and tracking [2]. SHRP 2 provides high-frequency video and telemetry from naturalistic driving, enabling analysis of driver behavior and risk factors [3]. BDD100K delivers large-scale annotated driving videos across diverse weather, lighting, and locations [4]. Brain4Cars focuses on driver maneuver anticipation using both in-cabin and exterior views [5]. However, these naturalistic datasets lack controlled environments, which may limit experimental consistency in certain research settings.

In perception evaluation, metrics such as precision, recall, F1 score, mAP, and mIoU remain widely used, though they treat each detection independently. Extensions to these metrics have addressed temporal aspects; for instance, Zhang et al. [6] enhance mAP with stability components for video detection, while Mao et al. [7] propose the Average Delay (AD) metric to capture detection latency under false alarm constraints. While these improvements consider temporal dynamics, PCD uniquely emphasizes distance-dependent reliability and fluctuations in detection confidence, providing a metric specifically suited for evaluating perception in ADS/ADAS contexts.

3 SensorRainfall Dataset

The SensorRainfall dataset was developed under both controlled and dynamic test environments to assess the impact of rainfall intensity on sensor performance. It quantifies key performance metrics such as detection probability, state estimation accuracy, and sensor-specific variables across different sensor modalities. This dataset is particularly valuable for analyzing the influence of precipitation on perception capabilities and overall system-level performance of ADAS and ADS.

The dataset contains object-level annotations for each sensor type, including camera, LiDAR, and radar. Data collection was conducted on the Virginia Smart Roads, a facility capable of simulating diverse weather conditions—including rainfall—across a 200-meter test track [8]. The testing scenario emulated Forward Collision Warning (FCW) and Automatic Emergency Braking (AEB) systems. Two environmental conditions were recorded: Clear Daylight and Rainy Daylight, the latter featuring a controlled rainfall rate of 64 mm/h [9].

The captured data comprises sequential front-view images of a target object—a red sedan—recorded at varying distances under different weather conditions. All images were taken from the ego vehicle at a resolution of 1920×1080 . Figure 2 presents representative sample images, and Table 1 provides a summary of the key statistical characteristics of the SensorRainFall dataset.



Figure 2: SensorRainfall Data Example.

Table 1: SensorRainfall dataset overview.

Scenario	Number of images	Distance between the ego vehicle and the red sedan (m)				
		mean	std	min	median	max
Clear daylight	278	107.989	61.852	5.553	105.976	214.247
Rainy daylight	317	122.251	69.800	5.476	121.208	240.669

To obtain the IoU for each perception benchmark, experienced and trained researchers manually reviewed each image and annotated the red sedan with a ground truth bounding box. The ground truth annotations include the coordinates of the top-left and bottom-right corners of the bounding box.

4 Perception Characteristics Distance

The PCD is a novel evaluation metric that quantifies the maximum distance at which a perception system can detect target objects with statistically significant reliability. Figure 3 illustrates the overall methodology for determining the PCD. This section begins by clarifying the concepts of IoU and

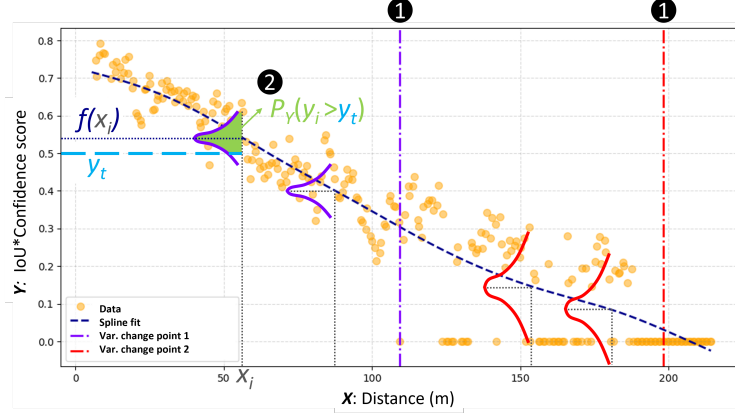


Figure 3: Illustration of the PCD identification process. The horizontal axis X represents the distance between the ego vehicle and the target object, while the vertical axis Y denotes the $\text{IoU} \times \text{confidence}$ score. The first step is to detect all points along the X -axis where the variance of Y changes significantly, marking segment boundaries. In the second step, for each distance x_i , the corresponding y_i is modeled as a Gaussian random variable $y_i \sim \mathcal{N}(\mu_i, \sigma_i^2)$, where the μ_i is given by the spline fit $f(x_i)$ and the σ_i is estimated from data within each segment. The probability $P_Y(y_i > y_t)$ is then computed based on a predefined detection quality threshold y_t . The PCD is defined as the maximum distance x_i for which the probability $P_Y(y_i > y_t)$ remains greater than a predefined probabilistic threshold p_t .

confidence score, and explains the rationale for using their product— $\text{IoU} \times \text{confidence}$ —as a more informative metric than either component alone. It then introduces a formal method for detecting significant variance change points in a univariate data distribution, enabling estimation of the confidence distribution at each individual distance point. Building on this foundation, the section concludes with a detailed procedure for determining the PCD of a given perception system.

4.1 $\text{IoU} \times \text{Confidence}$ score

PCD is computed using the product of two key metrics—IoU and confidence score—across varying distances. This combined measure captures both detection accuracy and certainty, providing a more informative indicator of perception performance than confidence alone. The IoU quantifies the accuracy of predicted object boundaries, which is computed by

$$\text{IoU} = \frac{|A \cap B|}{|A \cup B|} \quad (1)$$

where A is predicted bounding box, B is ground truth bounding box, $|A \cap B|$ is area of the intersection of A and B , and $|A \cup B|$ is the area of the union of A and B . An IoU ranges from 0 to 1, where 1 indicates perfect alignment. In object detection tasks, IoU is critical for determining whether a prediction is correct, often with a threshold (e.g., $\text{IoU} \geq 0.5$) used to classify a detection as a true positive.

The detection confidence score reflects a perception system’s estimated probability that a detected object truly exists, while IoU measures the spatial alignment between predicted and ground truth bounding boxes. Confidence score alone captures detection certainty but ignores localization accuracy. To address this, the $\text{IoU} \times \text{confidence}$ score is used, integrating both aspects to provide a more robust basis for evaluating perception reliability—especially in dynamic environments where accurate localization is essential.

4.2 Detection of variance change points

To estimate the variance of $\text{IoU} \times \text{confidence}$ score at each distance point, it is necessary to identify segments where the variance remains approximately constant. This requires detecting variance change points—specific locations in the sequential data where the variance shifts significantly [10].

These change points partition the data into segments with distinct levels of volatility. Detecting them typically involves first modeling the mean structure of the data using regression techniques [11], allowing the underlying variance pattern to be isolated and analyzed more accurately.

Splines are particularly effective for this initial regression fitting due to their ability to adaptively capture non-linear patterns without imposing rigid parametric assumptions. Unlike fixed-form linear models, spline regression decomposes the predictor space into locally smooth polynomial segments joined at optimized knot locations, ensuring mean estimation in complex temporal or spatial relationships. This flexibility prevents residual variances from being distorted by unmodeled curvature in the mean structure, a critical prerequisite for reliable variance change detection.

For $(x_i, y_i), i = 1, \dots, n$. A smoothed function $f(\cdot)$ can be estimated using spline regression such that

$$y_i = f(x_i) + \epsilon_i \quad (2)$$

where $\epsilon_i, i = 1, \dots, n$ denotes the independent random error with variance σ_i^2 . We seek to detect a variance change point x_τ such that $\sigma_1 = \sigma_2 = \dots = \sigma_\tau \neq \sigma_{\tau+1} = \dots = \sigma_n$.

Penalized splines [12] are particularly useful for variance change detection because they provide a flexible and smooth estimate of the mean structure. The smoothness is controlled by selecting an appropriate order of B-spline base functions, usually order three is enough [13]. Furthermore, penalized splines prevent overfitting by introducing a regularization parameter λ . The unknown regression function $f(\cdot)$ is estimated as a linear combination of coefficients and B-spline base functions,

$$f(x_i) = \sum_{j=1}^K \beta_j B_j(x_i) \quad (3)$$

where K is the pre-selected number of B-splines, $\beta_j, j = 1, \dots, K$ are the coefficients, and $B_j(\cdot)$ is the j th B-spline base function. In this paper, we select $K=10$ and B-spline base functions with order three to ensure smoothness over the second derivative. The function $f(\cdot)$ can be estimated by optimizing over the following regularized likelihood

$$\sum_{i=1}^n [y_i - \sum_{j=1}^K \beta_j B_j(x_i)]^2 + \lambda \sum_{j=3}^K (\Delta^2 \beta_j)^2 \quad (4)$$

where $\Delta^2(\cdot)$ denotes the second order difference, and $\lambda = 0.6$ is a pre-selected penalty parameter which suffices in our case. To select an appropriate λ for any other specific data, one can use cross-validation with AIC or BIC [14] criteria.

To test the existence of a variance change point, construct the following hypothesis

$$H_0 : \sigma_1 = \dots = \sigma_n \text{ v.s. } H_1 : \sigma_1 = \sigma_2 = \dots = \sigma_\tau \neq \sigma_{\tau+1} = \dots = \sigma_n \quad (5)$$

Considering the following likelihood [15] on a point $\tau = 1, \dots, n$,

$$l(\tau) = \tau \log \left\{ \frac{1}{\tau} \sum_{i=1}^{\tau} [y_i - f(x_\tau)]^2 \right\} + (n - \tau) \log \left\{ \frac{1}{n - \tau} \sum_{i=\tau+1}^n [y_i - f(x_\tau)]^2 \right\} \quad (6)$$

a test statistic T_n can be constructed based on the Schwartz information criterion (SIC) [16],

$$T_n = \log n - \min_{1 < \tau < n} \{l(x_\tau) - l(x_n)\} \quad (7)$$

Given α as our significance level, we reject H_0 if

$$a_n (\log n)^{1/2} T_n - b_n \log(n) > -\log\{-\log(1 - \alpha)/2\} \quad (8)$$

where $a_n = [2\log(\log(n))]^{1/2}/\log(n)$ and $b_n = \{2\log(\log(n)) + \frac{1}{2}\log[\log(\log(n))]\} - \log(\Gamma(\frac{1}{2}))/\log(n)$.

To detect all variance change points, we adopt a sequential hypothesis testing framework. The process begins by identifying the first significant change point x_{τ_1} using the entire dataset. Once x_{τ_1} is detected, the data is split into two segments: $[x_1, x_{\tau_1}]$ and $[x_{\tau_1+1}, x_n]$. Hypothesis testing is then applied to each segment independently to detect additional change points, such as x_{τ_2} and x_{τ_3} , if present. This iterative procedure continues until no further significant change points are found. By progressively narrowing the search intervals, the method avoids overlapping variance regimes and ensures that each structural break is accurately and independently identified.

4.3 Computation of Perception Characteristics Distance

As illustrated in Figure 3, the dynamic determination of PCD begins by analyzing the $\text{IoU} \times \text{confidence}$ score across distance and identifying all significant variance change points, denoted as $x_{\tau_1}, x_{\tau_2}, \dots, x_{\tau_M}$. These change points divide the data into segments exhibiting distinct statistical properties. Within each segment (i.e., between two consecutive change points), the $\text{IoU} \times \text{confidence}$ score, denoted as y_i , is assumed to follow a normal distribution:

$$y_i \sim \mathcal{N}(\mu_i, \sigma_i^2); \mu_i = f(x_i), \sigma_i = \text{std}(y_A) \quad (9)$$

where μ_i is modeled by a spline regression function $f(\cdot)$, σ_i is estimated by the standard deviation (std) of points in segment $A = \{j | \tau_m \leq j \leq \tau_{m+1}, m = 1, 2, \dots, M - 1\}$. The PCD is defined as the maximum distance x_i where the probability that y_i exceeds a detection quality threshold y_t is above a probabilistic threshold p_t :

$$PCD = \max\{x_i | P_Y(y_i > y_t) > p_t\} \quad (10)$$

In this formulation, PCD incorporates both the expected detection quality μ_i , and the associated uncertainty, represented by σ_i . By adapting to local statistical variations through identified variance change points, PCD establishes a principled, probabilistic cutoff distance beyond which the perception system can no longer be considered reliable.

In practical usage, users can adjust the thresholds y_t and p_t based on their specific detection requirements. For applications requiring higher perception quality, a larger y_t or higher p_t may be chosen. Conversely, in more tolerant scenarios, users may lower these values to extend the PCD while accepting reduced precision.

To comprehensively evaluate the perception system across varying thresholds, we compute the volume under the PCD surface over combinations of p_t and y_t . This aggregated metric is referred to as the mean PCD (mPCD). Similar to how AUC summarizes classifier performance by calculating the area under the ROC curve—plotting the true positive rate against the false positive rate across different thresholds—mPCD captures the overall perception characteristics of the perception system across ranges of two thresholds.

5 Experiments

This section presents a series of experiments designed to evaluate the effectiveness of various object detection models using the proposed PCD metric. The section begins implementation details, followed by a comprehensive analysis of the experimental results. This includes the detection of variance change points based on the $\text{IoU} \times \text{confidence}$ score, assessment of model performance through PCD, and examination of the impact of varying threshold settings on PCD outcomes.

5.1 Implement

Using the SensorRainFall dataset, a series of perception benchmarks were conducted focusing on detecting a red sedan across sequential images captured under two conditions: clear daylight and rainy daylight. Bounding boxes were annotated for each frame to evaluate model performance across environmental variations. Five object detection models were evaluated: Deformable DETR [17], Grounding DINO [18], DyHead [19], YOLOX [20], and GLIP [21]. Among these, GLIP and Grounding DINO are multi-modal models, while the others are deterministic. All models selected have demonstrated state-of-the-art performance on widely used open-source benchmarks such as Microsoft COCO [22] and Objects365 [23].

The following configurations are used for each model. Deformable DETR employs a ResNet-50 backbone with a two-stage refinement for improved region proposal generation. Grounding DINO utilizes a Swin-B backbone with 128 embedding dimensions, 18 layers in the third stage, a window size of 12, drop path rate of 0.3, and a modified neck to accommodate high-dimensional inputs (256/512/1024). DyHead integrates an ATSS detector with a Swin Transformer backbone, a combined FPN-DyHead neck, and is pretrained on ImageNet-22K and COCO with multi-scale augmentation. YOLOX uses a CSPDarknet backbone (deepen factor: 0.33, widen factor: 0.5), a YOLOXPAFPN neck with 128 output channels, and a YOLOXHead, trained on the COCO dataset with extensive augmentation. GLIP features a Swin-S backbone with 192 embedding dimensions,

a modified FPN neck, and an enhanced bounding box head incorporating early fusion and eight dynamic head blocks.

All perception benchmarks perform object detection directly on the SensorRainfall dataset without any fine-tuning. For GLIP and Grounding DINO, the text prompt "car" is used to guide the object detection task. During inference, no confidence score threshold is applied; instead, each model outputs the bounding box labeled "car" with the highest confidence score.

The software environment was based on Python 3.11 running on Rocky Linux 9.3. The model was trained on a high-performance GPU workstation with dual Intel Xeon Gold 6442 CPUs @ 2.60 GHz, 512 GB RAM, and one Nvidia Tesla H100 80 GB GPU.

5.2 Results

5.2.1 Variance change point of $\text{IoU} \times \text{Confidence score}$

Table 2 summarizes the detected variance change points of $\text{IoU} \times \text{Confidence score}$ across all benchmark models under both clear and rainy daylight conditions. All models but YOLOX exhibited more variance change points in rainy daylight compared to clear daylight, implying reduced stability and reliability in adverse weather. Deformable DETR demonstrated the largest increase in detected change points, rising from zero to three under rain, suggesting greatest sensitivity to environmental shifts.

Table 2: Detected Variance Change Points Across All Benchmarks ($\alpha = 0.05$). The upward or downward arrow indicates whether the model’s performance in rainy daylight improved or declined compared to clear daylight.

Model	Number of variance change points	x_{τ_1} (m)	x_{τ_2} (m)	x_{τ_3} (m)	x_{τ_4} (m)
Clear daylight					
Deformable DETR	0	–	–	–	–
Grounding DINO	2	29.407	154.556	–	–
DyHead	2	109.377	198.193	–	–
YOLOX	3	36.513	133.427	170.522	–
GLIP	2	81.399	154.556	–	–
Rainy daylight					
Deformable DETR	3↑	130.054	189.140	198.106	–
Grounding DINO	4↑	81.681	87.833	190.611	217.114
DyHead	4↑	16.037	84.795	195.101	208.407
YOLOX	3	119.157	138.339	153.980	–
GLIP	3↑	41.514	110.335	158.641	–

Figure 4 illustrates variance change points of Grounding DINO. Under clear daylight, the $\text{IoU} \times \text{confidence score}$ declines smoothly with distance, while in rainy conditions, the curve exhibits four change points, indicating fluctuating performance. These points x_τ segment the perception range into regions with distinct characteristics. For example, in $[0, 29.407]$, the model maintains high confidence and low variance, indicating stable detection. In contrast, the range $[87.833, 190.611]$ shows moderate scores with high variance, reflecting instability. Beyond 217.114, detection fails entirely, with scores dropping to zero.

5.2.2 Evaluation based on Reliable Perception Distance

Figure 5 presents the PCD of Grounding DINO under different weather conditions. With a threshold combination of $p_t = 0.5$ and $y_t = 0.5$, the PCD in clear daylight (94.776 m) is greater than that in rainy daylight (71.439 m), indicating that adverse weather conditions can reduce the reliable detection range of Grounding DINO.

In Table 3, in addition to mPCD, seven standard evaluation metrics were computed: mean $\text{IoU} \times \text{confidence score}$, mAP, AP50, AP75, and size-specific metrics (AP_S , AP_M , AP_L), with object sizes defined by bounding box area. The results show that mPCD effectively captures the maximum distance at which each model maintains reliable detection across varying thresholds of y_t and p_t . Models like Deformable DETR and Grounding DINO, which achieve higher mPCD in clear daylight,

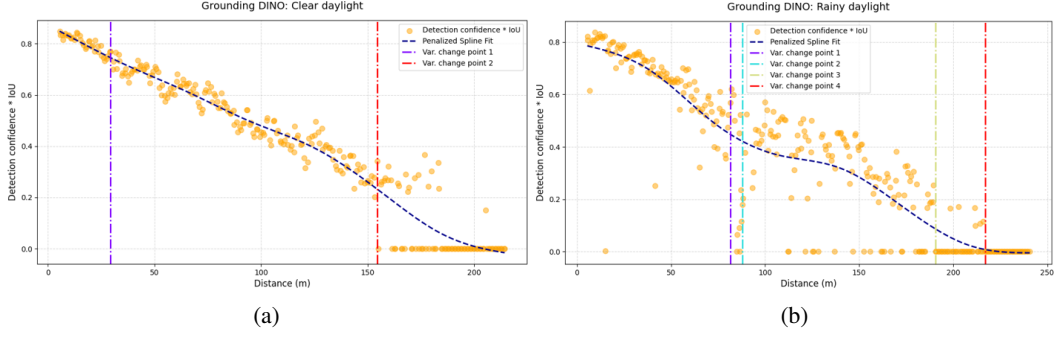


Figure 4: Detected variance change points under different weather conditions (Grounding DINO).

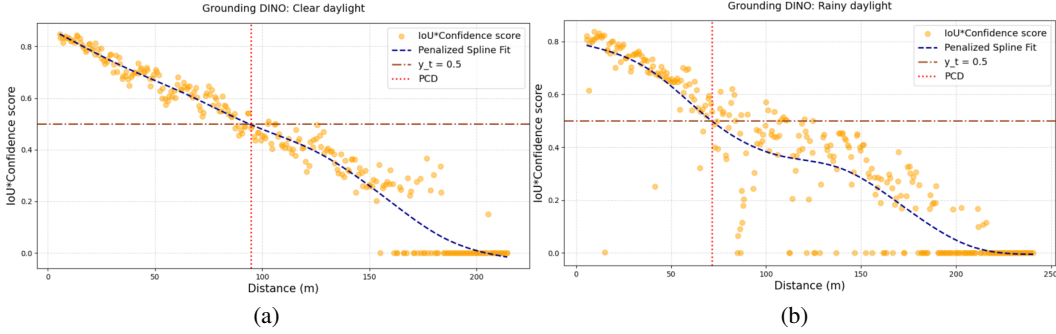


Figure 5: PCD of Grounding DINO under Various Weather Conditions (threshold: $p_t = 0.5$ and $y_t = 0.5$).

also perform well on traditional metrics, indicating alignment between spatial reliability and detection quality. However, mPCD reveals differences not captured by mAP—for instance, although DyHead and Grounding DINO have similar mAP scores, Grounding DINO consistently achieves a higher mPCD, highlighting its superior range reliability. This demonstrates the added value of mPCD for real-world applications where perception performance over distance is critical.

Table 3: Evaluation results of perception benchmarks. mPCD refers to the mean of the PCDs across threshold combinations of y_t and p_t .

Model	mPCD (m)	Mean of IoU \times Confidence score	mAP	AP ₅₀	AP ₇₅	AP _S	AP _M	AP _L
Clear daylight								
Deformable DETR	106.275	0.487	0.548	0.953	0.510	0.934	0.982	0.956
Grounding DINO	92.783	0.425	0.564	0.780	0.618	0.691	0.982	0.956
DyHead	73.110	0.337	0.560	0.744	0.640	0.641	0.982	0.956
YOLOX	72.794	0.336	0.448	0.625	0.478	0.474	0.982	0.956
GLIP	62.864	0.257	0.438	0.528	0.489	0.338	0.982	0.956
Rainy daylight								
Deformable DETR	57.224↓	0.249↓	0.367↓	0.583↓	0.372↓	0.491↓	0.777↓	0.846↓
Grounding DINO	86.593 ↓	0.354 ↓	0.484 ↓	0.684 ↓	0.526 ↓	0.565 ↓	0.984 ↑	0.923 ↓
DyHead	66.010↓	0.274↓	0.468↓	0.634↓	0.533↓	0.500↓	0.984 ↑	0.884↓
YOLOX	52.426↓	0.208↓	0.323↓	0.413↓	0.353↓	0.223↓	0.857↓	0.923 ↓
GLIP	42.591↓	0.166↓	0.288↓	0.328↓	0.324↓	0.083↓	0.936↓	0.923 ↓

5.2.3 Effects of various thresholds on Reliable Perception Distance

Figure 6 shows the PCD of Grounding DINO under clear and rainy daylight across threshold combinations of p_t and y_t (ranging from 0.1 to 0.9). In clear conditions, PCD transitions smoothly, with detection distances from 6m to 214m, peaking when both thresholds are low. In contrast, rainy conditions exhibit abrupt changes in PCD, indicating greater sensitivity to threshold variation. For nearly all threshold pairs, PCD values are higher in clear daylight, consistent with trends observed in traditional evaluation metrics.

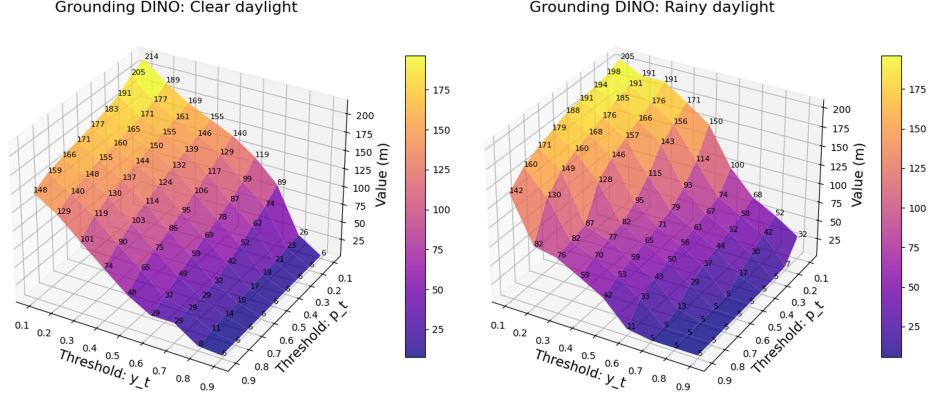


Figure 6: Effects of various threshold combination of p_t and y_t on PCD (Grounding DINO).

The selection of appropriate p_t and y_t presents a fundamental trade-off between detection range and reliability. Lower thresholds ($p_t, y_t \approx 0.1-0.3$) maximize detection distance but potentially include less reliable detections, while higher thresholds ($p_t, y_t \approx 0.6-0.9$) ensure greater confidence at the cost of substantially reduced detection range. For practical applications, balanced threshold values ($p_t \approx 0.4-0.6$, $y_t \approx 0.4-0.6$) provide moderate detection distances (90-120 meters in clear conditions, 80-110 meters in rainy conditions) while maintaining reasonable detection reliability. These moderate thresholds offer robustness across varying environmental conditions while avoiding the extremes of either overly permissive or restrictive detection criteria.

6 Conclusion

This study introduces the SensorRainFall dataset—a controlled collection capturing perception performance under clear and rainy conditions—and demonstrates that detection confidence scores over distance exhibit heteroscedastic variance, revealing limitations of traditional static metrics. We develop a statistical approach to estimate the mean and variance of confidence as a function of distance and propose the PCD metric, which defines the maximum range at which a perception system maintains confidence consistency above a certain threshold. Through extensive experiments on multiple state-of-the-art object detectors using the SensorRainFall dataset, we validate that PCD offers a more robust and informative evaluation of perception stability in dynamic, real-world scenarios; however, our evaluation is currently limited to object detection on SensorRainFall, and future work should extend PCD’s application to other datasets and perception tasks. By improving the reliability assessment of perception systems, PCD can ultimately enhance autonomous-driving safety, though accelerated adoption of full autonomy may also disrupt driving-related employment.

References

- [1] Holger Caesar, Varun Bankiti, Alex H Lang, Sourabh Vora, Venice Erin Liong, Qiang Xu, Anush Krishnan, Yu Pan, Giancarlo Baldan, and Oscar Beijbom. nuscenes: A multimodal dataset for autonomous driving. In *Proceedings of the IEEE/CVF conference on computer vision and pattern recognition*, pages 11621–11631, 2020.
- [2] Andreas Geiger, Philip Lenz, Christoph Stiller, and Raquel Urtasun. Vision meets robotics: The kitti dataset. *International Journal of Robotics Research (IJRR)*, 2013.

- [3] Jonathan M Hankey, Miguel A Perez, and Julie A McClafferty. Description of the shrp 2 naturalistic database and the crash, near-crash, and baseline data sets. Technical report, Virginia Tech Transportation Institute, 2016.
- [4] Fisher Yu, Haofeng Chen, Xin Wang, Wenqi Xian, Yingying Chen, Fangchen Liu, Vashisht Madhavan, and Trevor Darrell. Bdd100k: A diverse driving dataset for heterogeneous multitask learning. In *Proceedings of the IEEE/CVF conference on computer vision and pattern recognition*, pages 2636–2645, 2020.
- [5] Ashesh Jain, Hema S Koppula, Shane Soh, Bharad Raghavan, Avi Singh, and Ashutosh Saxena. Brain4cars: Car that knows before you do via sensory-fusion deep learning architecture. *arXiv preprint arXiv:1601.00740*, 2016.
- [6] Hong Zhang and Naiyan Wang. On the stability of video detection and tracking. *arXiv preprint arXiv:1611.06467*, 2016.
- [7] Huizi Mao, Xiaodong Yang, and William J Dally. A delay metric for video object detection: What average precision fails to tell. In *Proceedings of the IEEE/CVF International Conference on Computer Vision*, pages 573–582, 2019.
- [8] Tom Gibson. Virginia’s smart road: Where researchers make the extreme weather. *Weatherwise*, 68(4):20–27, 2015.
- [9] Jonathan B Cowan and Loren Stowe. Investigation of adas/ads sensor and system response to rainfall rate. Technical report, National Surface Transportation Safety Center for Excellence, 2024.
- [10] Douglas M Hawkins and KD Zamba. A change-point model for a shift in variance. *Journal of Quality Technology*, 37(1):21–31, 2005.
- [11] Heping Zhang Yue S. Niu, Ning Hao. Multiple change-point detection: A selective overview. *Institute of Mathematical Statistics*, 31(4):611–623, 2016.
- [12] Brian D. Marx Paul H. C. Eilers. Flexible smoothing with b-splines and penalties. *Statistical Science*, 11(2):89–121, 1996.
- [13] Brian D. Marx Paul H. C. Eilers. Splines, knots, and penalties. *WIREs Comp Stat*, 2(6):637–653, 2010.
- [14] Jayanta K. Ghosh Arijit Chakrabarti. Aic, bic and recent advances in model selection. *Handbook of the Philosophy of Science*, 7:583–605, 2011.
- [15] Zhenguo Gao, Zuofeng Shang, Pang Du, and John L. Robertson and. Variance change point detection under a smoothly-changing mean trend with application to liver procurement. *Journal of the American Statistical Association*, 114(526):773–781, 2019. doi: 10.1080/01621459.2018.1442341.
- [16] Gideon Schwarz. Estimating the dimension of a model. *Ann. Statist*, 6(2):461–464, 1978.
- [17] Xizhou Zhu, Weijie Su, Lewei Lu, Bin Li, Xiaogang Wang, and Jifeng Dai. Deformable detr: Deformable transformers for end-to-end object detection. In *International Conference on Learning Representations*, 2021. URL <https://openreview.net/forum?id=gZ9hCDWe6ke>.
- [18] Shilong Liu, Zhaoyang Zeng, Tianhe Ren, Feng Li, Hao Zhang, Jie Yang, Qing Jiang, Chunyuan Li, Jianwei Yang, Hang Su, Jun Zhu, and Lei Zhang. Grounding dino: Marrying dino with grounded pre-training for open-set object detection, 2024. URL <https://arxiv.org/abs/2303.05499>.
- [19] Xiyang Dai, Yinpeng Chen, Bin Xiao, Dongdong Chen, Mengchen Liu, Lu Yuan, and Lei Zhang. Dynamic head: Unifying object detection heads with attentions. In *Proceedings of the IEEE/CVF Conference on Computer Vision and Pattern Recognition (CVPR)*, 2021.
- [20] Zheng Ge, Songtao Liu, Feng Wang, Zeming Li, and Jian Sun. Yolox: Exceeding yolo series in 2021, 2021. URL <https://arxiv.org/abs/2107.08430>.

- [21] Liunian Harold Li, Pengchuan Zhang, Haotian Zhang, Jianwei Yang, Chunyuan Li, Yiwu Zhong, Lijuan Wang, Lu Yuan, Lei Zhang, Jenq-Neng Hwang, Kai-Wei Chang, and Jianfeng Gao. Grounded language-image pre-training, 2022. URL <https://arxiv.org/abs/2112.03857>.
- [22] Tsung-Yi Lin, Michael Maire, Serge Belongie, James Hays, Pietro Perona, Deva Ramanan, Piotr Dollár, and C Lawrence Zitnick. Microsoft coco: Common objects in context. In *Computer vision—ECCV 2014: 13th European conference, zurich, Switzerland, September 6-12, 2014, proceedings, part v 13*, pages 740–755. Springer, 2014.
- [23] Shuai Shao, Zeming Li, Tianyuan Zhang, Chao Peng, Gang Yu, Xiangyu Zhang, Jing Li, and Jian Sun. Objects365: A large-scale, high-quality dataset for object detection. In *Proceedings of the IEEE/CVF International Conference on Computer Vision (ICCV)*, October 2019.